Downloaded from orbit.dtu.dk on: Nov 01, 2026



DTU Library

Høje Taastrup Pit Thermal Energy Storage

2025 Measurement Report

Sifnaios, Ioannis; Jensen, Adam R.; Furbo, Simon

Link to article, DOI:
10.11581/b8e50bfb-49e8-4ff4-98a7-e8b90aa74ffd

Publication date:
2025

Document Version
Publisher's PDF, also known as Version of record

Link back to DTU Orbit

Citation (APA):
Sifnaios, I., Jensen, A. R., & Furbo, S. (2025). *Høje Taastrup Pit Thermal Energy Storage: 2025 Measurement Report*. Technical University of Denmark. https://doi.org/10.11581/b8e50bfb-49e8-4ff4-98a7-e8b90aa74ffd

General rights
Copyright and moral rights for the publications made accessible in the public portal are retained by the authors and/or other copyright owners and it is a condition of accessing publications that users recognise and abide by the legal requirements associated with these rights.

- Users may download and print one copy of any publication from the public portal for the purpose of private study or research.
- You may not further distribute the material or use it for any profit-making activity or commercial gain
- You may freely distribute the URL identifying the publication in the public portal

If you believe that this document breaches copyright please contact us providing details, and we will remove access to the work immediately and investigate your claim.

EUDP

Høje Taastrup Pit Thermal Energy Storage

2025 Measurement Report



VEKS

HØJE TAASTRUP fjernvarme amba

PlanEnergi

DTU

The FLEX_TES project was funded by EUDP under grant number 64018-0134.

Participants in the FLEX_TES project:

- Vestegnens Kraftvarmeselskab I/S (VEKS), Project leader, www.veks.dk
- Høje Taastrup Fjernvarme amba, www.htf.dk
- PlanEnergi, www.planenergi.dk
- EA Energianalyse, www.ea-energianalyse.dk
- Technical University of Denmark (DTU), www.dtu.dk

Report authors:

Ioannis Sifnaios (DTU)

Adam R. Jensen (DTU)

Simon Furbo (DTU)

Reviewers:

Niels From (PlanEnergi)

Finn Bruus (VEKS)

Front page image:

Ioannis Sifnaios

DOI: https://doi.org/10.11581/b8e50bfb-49e8-4ff4-98a7-e8b90aa74ffd

Contents

1	Høje Taastrup PTES design and operation	1
2	Overview of the monitoring system	1
3	Water temperatures and energy content	2
4	Water temperature profiles	4
5	Charge/discharge temperatures	6
6	Charge/discharge thermal power	7
7	Ground temperature	8
8	Lid temperature and humidity	8
9	Lid heat transfer coefficient (U-value)	10
10	Water pH measurements	11
11	Storage efficiency	12
12	Conclusion	13
13	References	13

1 Høje Taastrup PTES design and operation

Information regarding the design and implementation of the PTES in Høje Taastrup is provided in [1]. Details regarding the operation of the PTES in 2023 and 2024 is provided in [2] and [3].

2 Overview of the monitoring system

This report presents the measurement results of the pit thermal energy storage (PTES) in Høje Taastrup from January to December 2025. The storage performance has been monitored using various sensors, as shown in Figure 1 and Figure 2.

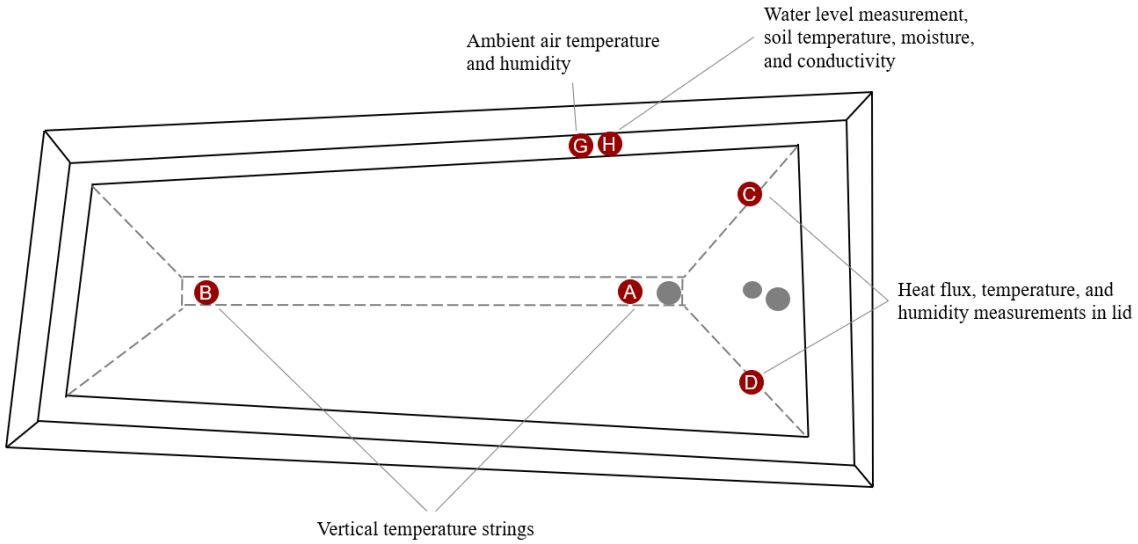


Figure 1: Top view of the installed measurement equipment and their locations.

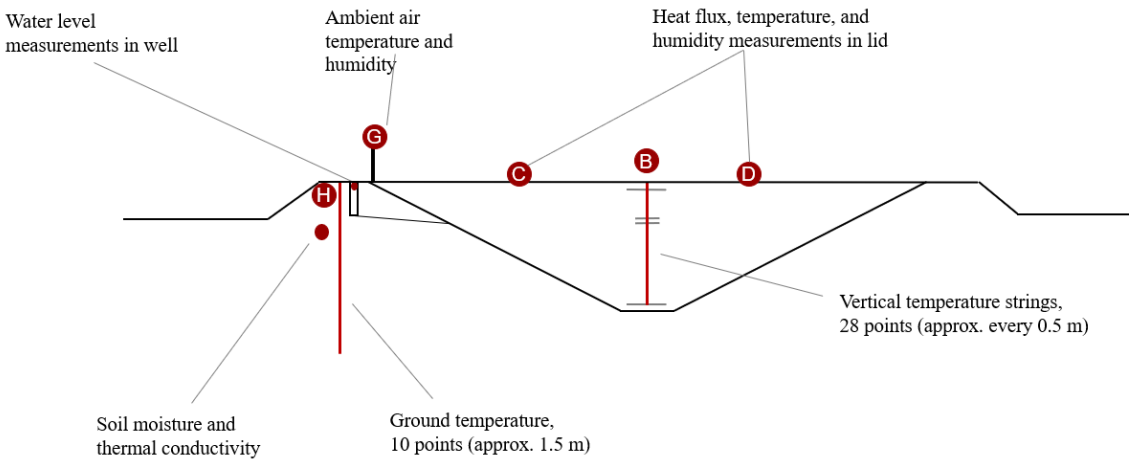


Figure 2: Side view of the installed measurement equipment and their locations.

The lid consists of two layers of XPS insulation, each with a thickness of 0.075 m, and two layers of NOMATEC insulation (previously called Nomalen), each with a thickness of 0.0625 m. Five temperature, two humidity, and one heat flux sensors were installed between the different layers of insulation in the lid at two different locations (C and D in Figure 1). The sensors were placed between the insulation layers, as shown in Figure 3.

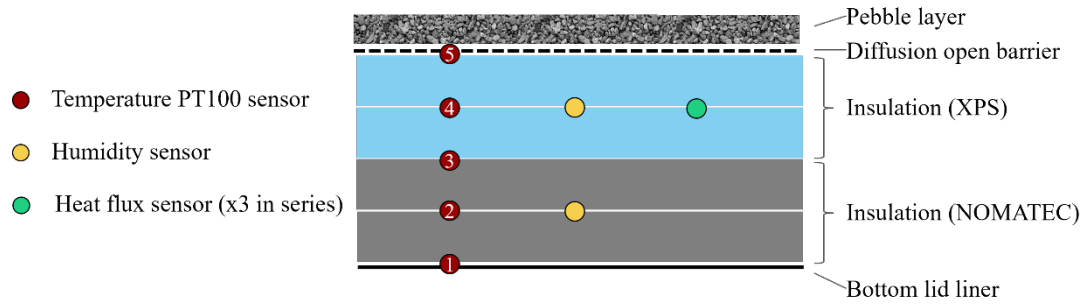


Figure 3: Cross-section of the PTES lid with the locations of the installed sensors.

3 Water temperatures and energy content

An error with the data logging occurred in 2025, resulting in data missing for most parameters during the summer of 2025. However, the operation of the storage can still be assessed, as all the essential parameters were logged.

The water temperature in the PTES was measured using four temperature strings with 14 sensors each, placed in locations A and B in Figure 1. The measurements are presented in Figure 4 (top). The temperature plot indicates that the PTES is slightly underutilized. Especially in the first half of 2025, the PTES was mainly used for charging/discharging small amounts of energy, which is not in line with the expected operation. However, it should be noted that the PTES conducted 10 full storage cycles in 2025 (compared to 9 in 2024) and that there are continuous efforts to increase the PTES utilization throughout the year.

The maximum capacity of the PTES (assuming a 100% utilization factor) is: $Q_{Max} = \rho \cdot V \cdot C_p \cdot \Delta T \approx 3300$ MWh.

Where $\rho = 965.4\ \mathrm{kg/m^3}$, $V = 70880\ \mathrm{m^3}$, $C_p = 4.19 \frac{\mathrm{kJ}}{\mathrm{kg\ K}}$, and $\Delta T = 41.5$ K (since the temperature operation range of the PTES is 48.5-90 °C).

Since the total discharged energy during the investigated period was 33626 MWh (see Table 4), the number of equivalent storage cycles for 2025 was: $N_{cycles} = E_{discharge}/Q_{Max} \approx 10$. It should be noted that a 100% utilization factor cannot be achieved in practice due to the boundary layer between the warm and cold water domains, and it is very hard to charge and discharge the storage fully. Typically, a utilization factor of 80-85% can be achieved.

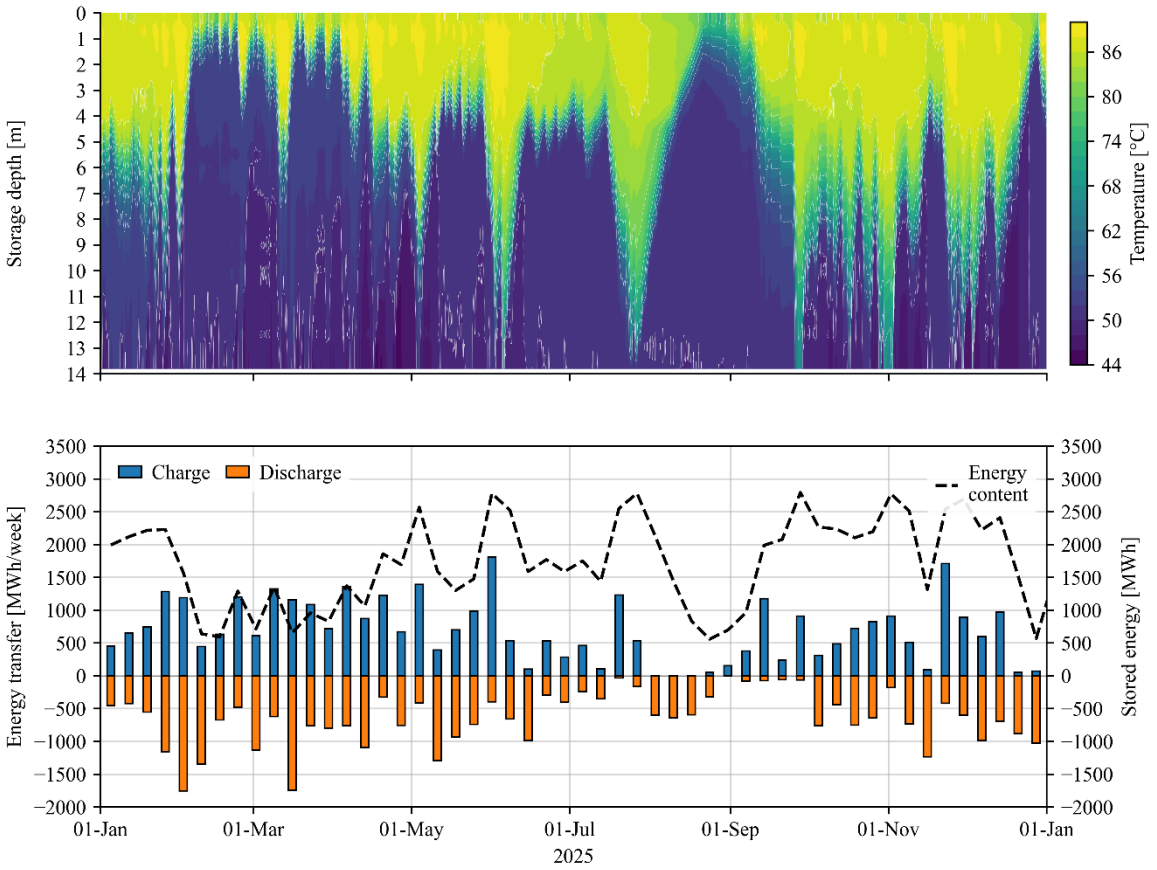


Figure 4: (top) Storage water temperature and (bottom) weekly charged, discharged energy and energy content (a reference temperature of 48.5 °C was used for calculating the energy content).

Another observation from Figure 4 (top) is that, similarly to previous years, the temperature of the top water layer was not maintained at a constant 90°C, as initially believed during the feasibility stage. Figure 5 shows the water temperature at the top of the PTES (under the lid) as a duration curve for 2025. The top layer water temperature was never measured higher than 90°C, while it was higher than 85 °C 78% of the time, and higher than 80°C 95% of the time. This operation is expected to positively affect the liner's lifetime.

The expected lifetime of the liner can be estimated using the cumulative damage approach, as suggested by G. Wallner [4]. As a rule of thumb, this method claims that the lifetime of a polypropylene (PP) liner is reduced by a factor of 1.7 when the temperature is increased by 10 K. The following calculations are based on the assumption that the liner has an expected lifetime of 20 years when exposed to 90 °C. The following equations were used to calculate the expected liner lifetime:

$$L(T_{top}) = 20 \cdot 1.7^{\frac{90-T_{top}}{10}}$$

$$L_{total} = \frac{1}{\sum_1^{8760} \frac{1}{8760 \cdot L(T_{top})}}$$

$$T_{eqv} = 90 - 10 \cdot \frac{\ln\left(\frac{L_{total}}{20}\right)}{\ln(1.7)}$$

where T_{top} is the temperature of the top water layer, L_{total} is the total expected lifetime of the liner, and T_{eqv} is the equivalent temperature of the liner. The equivalent temperature is the single constant temperature at which the polymer liner would experience the same total degradation over its lifetime as it does under the actual time-varying temperature conditions.

Table 1: Yearly mean and equivalent top water temperature in the PTES and expected liner lifetime.

Year	Top water mean temperature [°C]	Equivalent liner temperature [°C]	Expected total liner lifetime [years]
2023	84.9	84.8	26.3
2024	84.7	85.4	25.6
2025	86.2	86.4	24.2

Based on the values in Table 1, it can be seen that the mean water temperature under the lid was higher in 2025 compared to the previous years. If the storage was to operate under the same conditions as in 2025, then the expected total lifetime would be approximately 24 years.

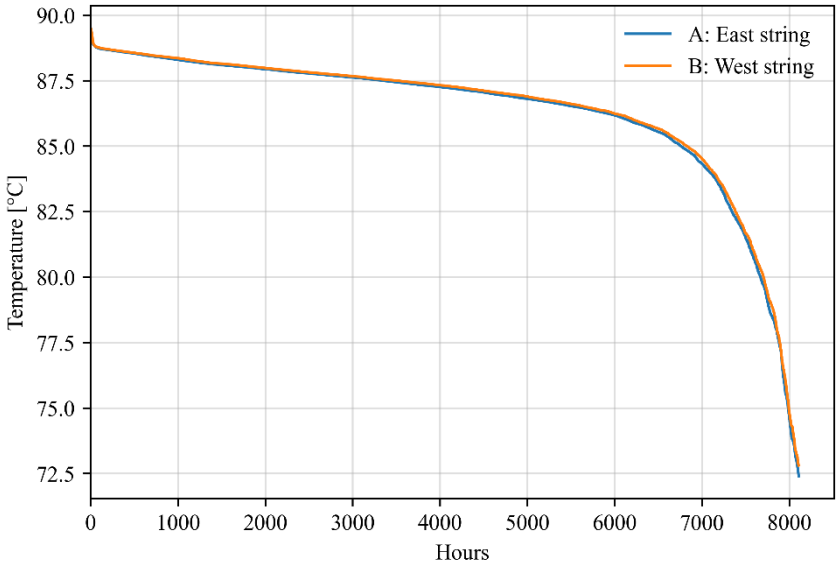


Figure 5: Duration curves for the water temperature under the lid for 2025.

4 Water temperature profiles

Vertical temperature stratification is essential, where water in the PTES is stored at different temperature levels, forming a vertical temperature gradient. A high degree of stratification indicates minimal mixing between layers. Figure 6 and Figure 7 present vertical temperature profiles in the PTES for the period May to June 2025 as a function of the storage height and volume, respectively. The reason for selecting this period is that, during this period, the

storage performed almost a full charge-discharge cycle (i.e., started relatively empty, then was almost fully charged, and then discharged). Notably, the temperature gradient is steeper during discharging than during charging. This is partly due to the lower flow rates during discharge and the tapered shape of the storage, where a 1-meter thermocline at the top during charging expands as it moves downward. Additionally, during discharge, the middle diffuser is mainly used for removing water at intermediate temperatures (i.e., between 90 and 50 °C), thus steepening the thermocline. However, although a steep thermocline is a good indicator of stratification, assessing stratification solely based on plots is not straightforward.

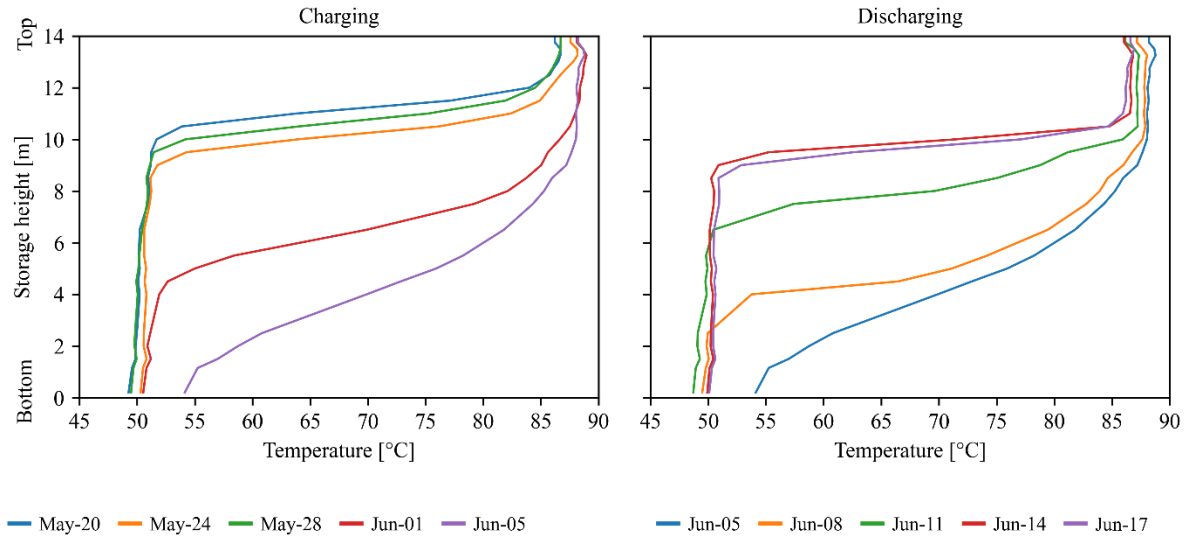


Figure 6: Temperature profiles in the storage for May-June 2025 as a function of the storage height.

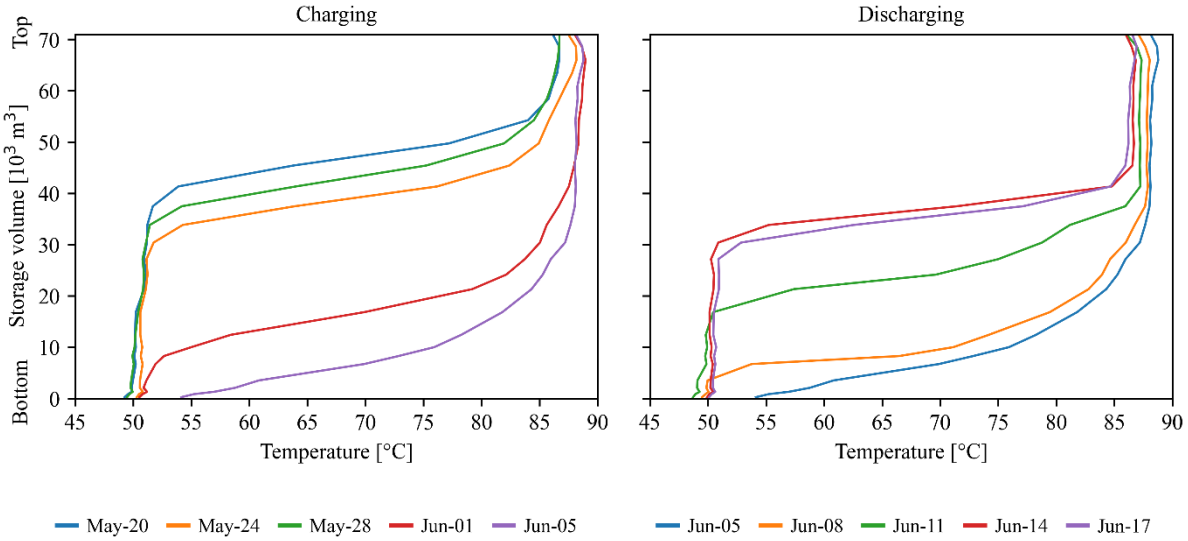


Figure 7: Temperature profiles in the storage for May-June 2025 as a function of the storage volume.

5 Charge/discharge temperatures

Table 2 presents the diffuser's weighted average temperature during charge and discharge, and the mean flow rates. Figure 8 and Figure 9 present the diffuser temperatures as a function of accumulated charged and discharged flow, respectively.

Table 2: Diffuser temperatures and flow rates during charging and discharging.

Operation	Diffuser	Weighted avg. temperature [°C]	Mean flow rate [m^3/hr]	Cumulative flow [10^3 m^3]
Charge	Top (in)	89.2	361	845
	Bottom (out)	50.3		
Discharge	Top (out)	85.4	125	414
	Middle (out)	79.2	138	459
	Bottom (in)	49.8	263	873

It can be observed that since the PTES is charged by Copenhagen's central transmission district heating network (which operates at around 110 °C), it was possible to charge the PTES with an almost constant temperature of 90 °C. It should be noted that although there had been some instances where the temperature of the top diffuser was higher than 90 °C during charging (see Figure 8), the temperature measured by the temperature strings in the water was never higher than 90 °C (see Figure 4(top) and Figure 5).

Additionally, it can be observed that the return temperature from the local district heating network was relatively high during 2025, with a mean bottom diffuser discharge temperature of approximately 50 °C. It should be noted that a minimum limit of 0.03 MW was applied to the charge and discharge operation, accounting for more than 99% of the operation time.

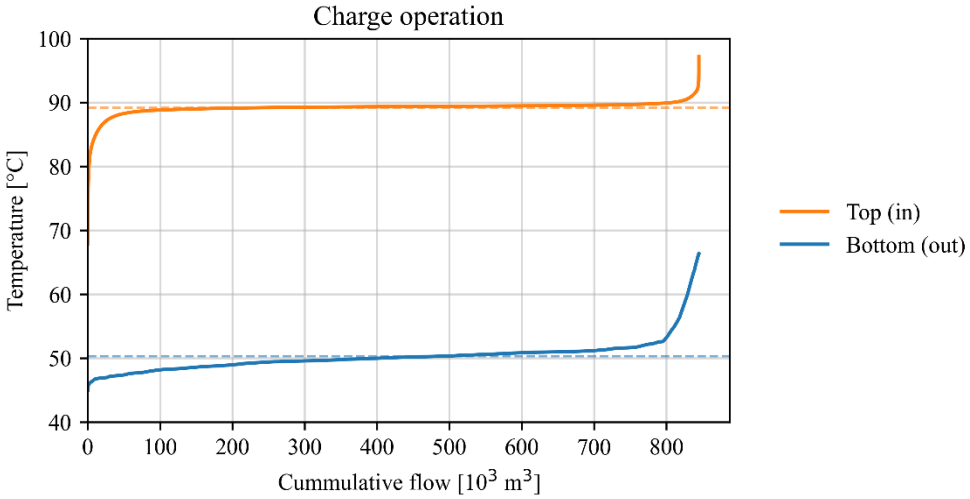


Figure 8: Top and bottom diffuser temperatures during charging. The dashed lines indicate the weighted mean temperatures.

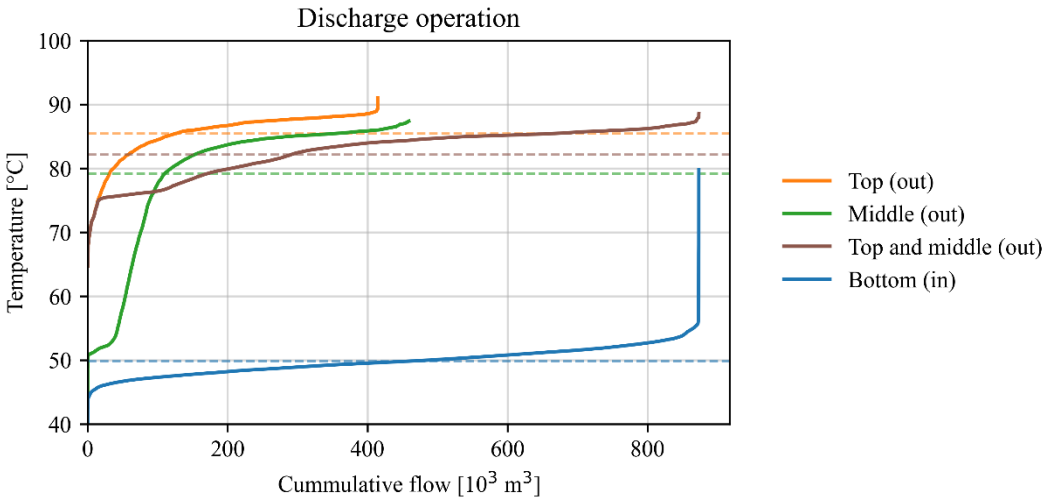


Figure 9: Top, middle, and bottom diffuser temperatures during discharging. The dashed lines indicate the weighted mean temperatures. The brown line is the calculated mixed temperature of the top and middle diffuser temperatures.

6 Charge/discharge thermal power

Similar to 2023 and 2024, limitations regarding the charge and discharge capacities remained in 2025. For example, the low heat demand of the local Høje Taastrup network led to limited discharging during the summer and autumn. However, it should be noted that the district heating grid of Høje Taastrup continues to expand, so the heat load is higher each year compared to the previous one. Figure 10 presents the duration curves of the charge/discharge thermal power of the PTES. The storage was designed with a maximum charge/discharge thermal power of 30 MW. On average, the charge thermal power for 2025 was 15 MW, while the mean discharge thermal power was 8.1 MW, both of which are higher compared to 2024.

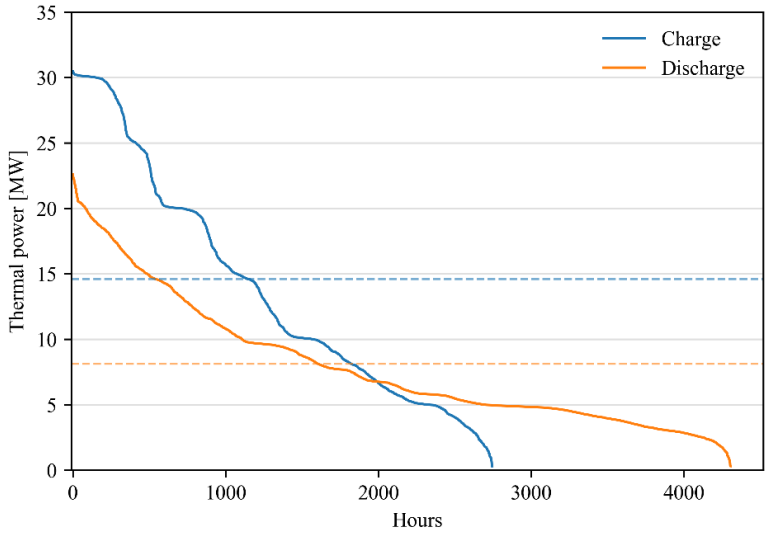


Figure 10: Duration curves of charged and discharged thermal power. Dashed lines indicate the mean values.

7 Ground temperature

The ground temperatures on the northern side of the PTES were measured using a string of 11 temperature sensors buried in the embankment. Figure 11 presents the measurements at different depths since the start of the data logging of the ground temperatures. It can be observed that due to the PTES operation, the ground temperatures have generally been increasing with time. This heating of the ground positively affects the PTES performance, as heat losses decrease with higher ground temperature. Nevertheless, the ground temperature close to the surface drops after September due to the low ambient temperatures.

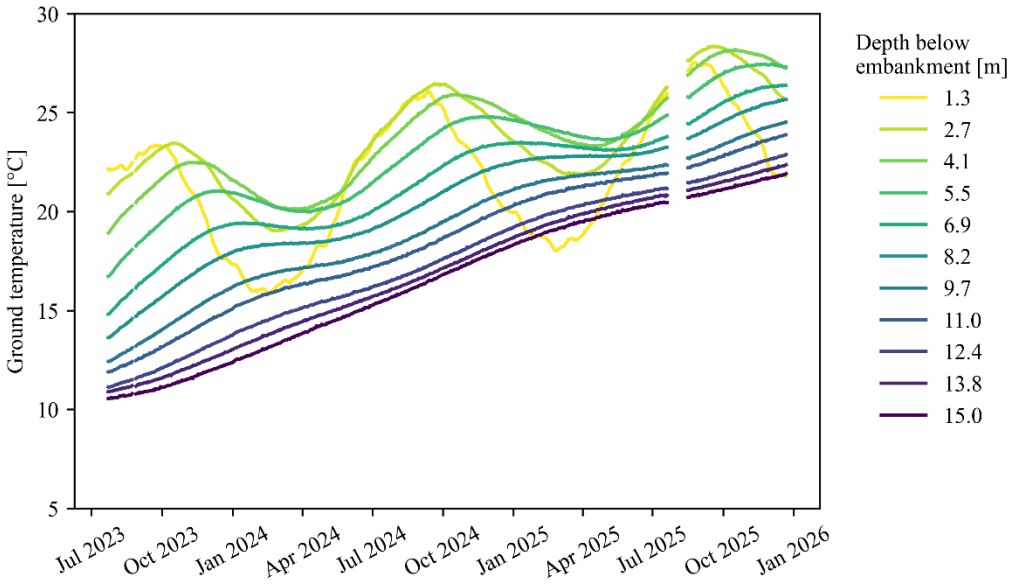


Figure 11: Soil temperatures at different depths measured on the northern side of the embankment.

8 Lid temperature and humidity

The temperature and humidity in the lid are presented in Figure 12 and Figure 13, respectively. The temperature of the top water layer, ambient air temperature, and humidity are also plotted for comparison. It should be noted that temperature and humidity in the lid are measured at two different locations (see Figure 1). The “bottom” sensor is closest to the storage water for both temperature and humidity sensors, while the “top” sensor is furthest from the storage water.

Although there is good agreement between the lid temperatures at the two locations, humidity measurements vary. This is most likely due to different drainage conditions between the insulation mats at the two locations and/or measurement uncertainty of the sensors. Nevertheless, it can be observed that, in both measurement locations, there is more absolute moisture (but less relative humidity) between the two NOMATEC insulation layers (bottom) than between the two XPS layers (top). It should be noted that some rainwater drainage issues were identified in 2025, due to the issues with the sensors controlling the rainwater-removing pumps. This issue is possibly the cause of the high humidity in the lid in the fall of 2025. This problem was corrected in late 2025.

It should be noted that the bottom humidity sensor at location D seems to measure a constant value close to zero after the fall of 2025. This is likely due to a sensor failure; however, it is unclear whether this is a permanent issue. The mean yearly humidity values for the two measurement locations in the lid are presented in Table 3.

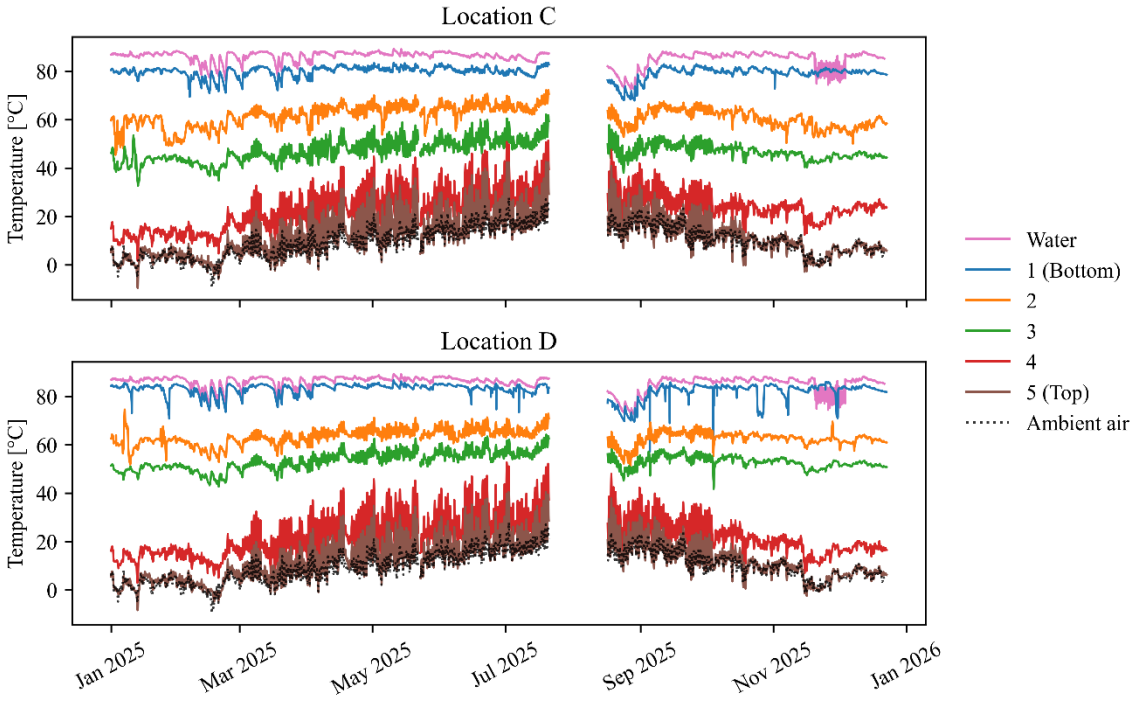


Figure 12: Temperature levels inside the lid at the two measurement locations.

Table 3: Mean humidity yearly values for the measured locations in the lid.

Humidity type	Location	Top of lid	Bottom of lid	Ambient
Relative	C D	59 % 56 %	21 % 38 %	86 %
Absolute	C D	1.3 g/m^3 1.1 g/m^3	3.0 g/m^3 5.9 g/m^3	0.8 g/m^3

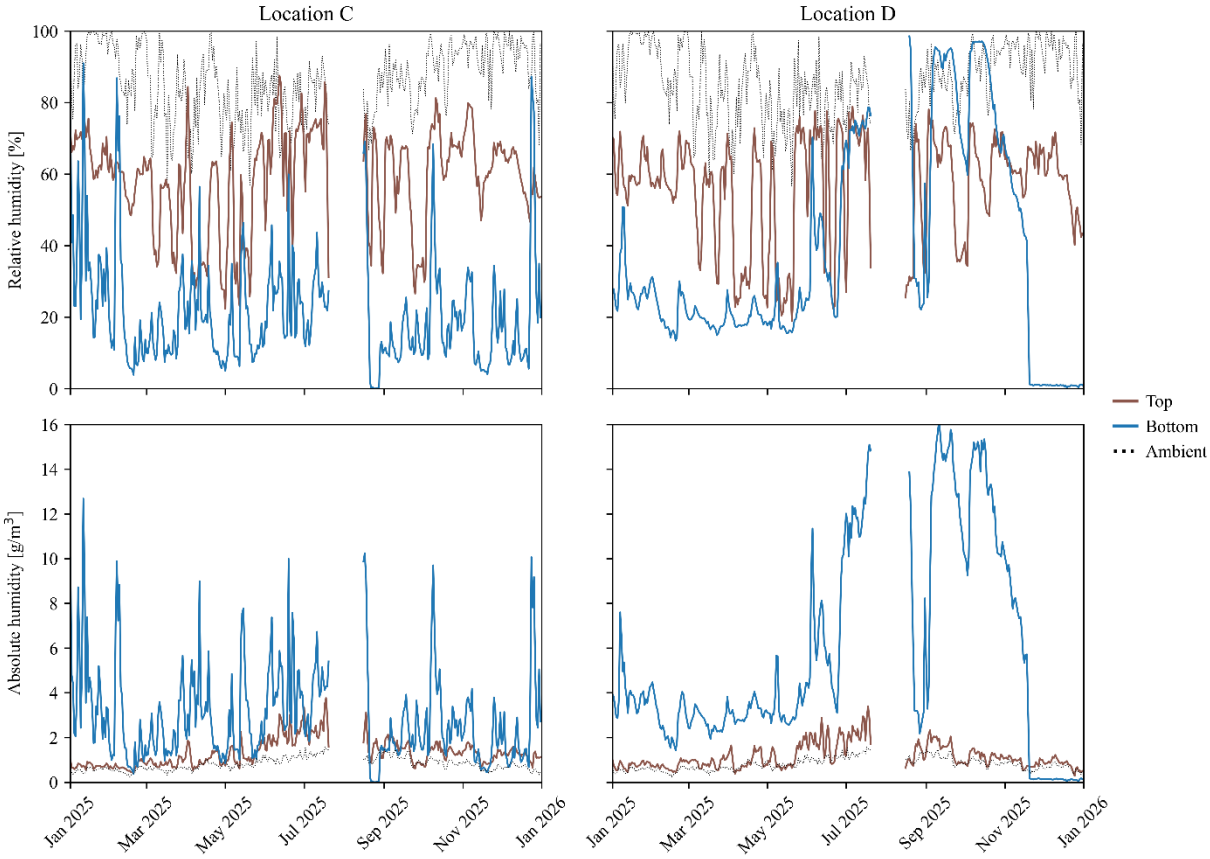


Figure 13: Humidity levels inside the lid at the two measurement locations.

9 Lid heat transfer coefficient (U-value)

The measured and theoretically calculated heat transfer coefficient (U-value) of the lid is presented in Figure 14. The theoretical U-value (0.151 W/(m^2 K)) is indicated with a dashed line and was calculated from the insulation's thermal characteristics determined from laboratory tests:

- The NOMATEC thickness is 0.0625 m per layer with thermal conductivity of 0.0483 W/(m K) at 82 °C and 0.0462 W/(m K) at 66 °C.
- The XPS thickness is 0.075 m per layer with thermal conductivity of 0.0397 W/(m K) at 46 °C and 0.0358 W/(m K) at 22 °C.

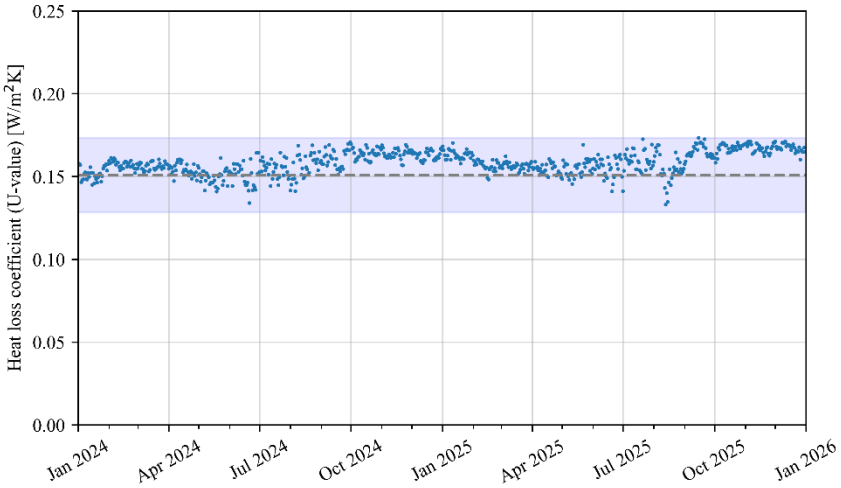


Figure 14: Daily average lid heat transfer coefficient (blue dots). The shaded area indicates a ±10% difference from the theoretical value.

The U-value is determined based on the measured heat flux, the top water layer temperature, and the ambient air temperature. Since the heat flux is measured in two locations on the lid, the average value of the two measurements was used. It should be noted that the measured U-value is generally higher than the theoretical value. However, the measured value is always within ± 10% of the theoretical value (blue-shaded area). Somewhat higher heat loss is to be expected due to thermal bridges and moisture in the insulation. It should be noted that no correlation was found between the lid humidity or lid temperature and the lid U-value.

10 Water pH measurements

The water pH measurements conducted in 2025 are shown in Figure 15. The pH is continuously measured using a sensor (blue curve) and by manually extracting water from the storage at different depths (red dots). Note that the red dots are the average values at the different depths. It is essential to maintain the storage water pH at approximately 10 to prevent corrosion in the metal parts (e.g., diffusers and connection pipes). The sensor measurements at the start of 2025 differed significantly from the manual pH measurements. In early summer 2025, there was an effort to improve the sensor operation, which can also be observed in Figure 15, since the sensor was in better agreement with the manual measurements. However, it can be observed that although the manual measurements indicate the pH was maintained at the desired level, the sensor does not agree with the manual measurements, suggesting that conducting continuous pH measurements is not straightforward. The manual measurements are considered the most accurate, as there have been known issues with the operation of the pH sensor.

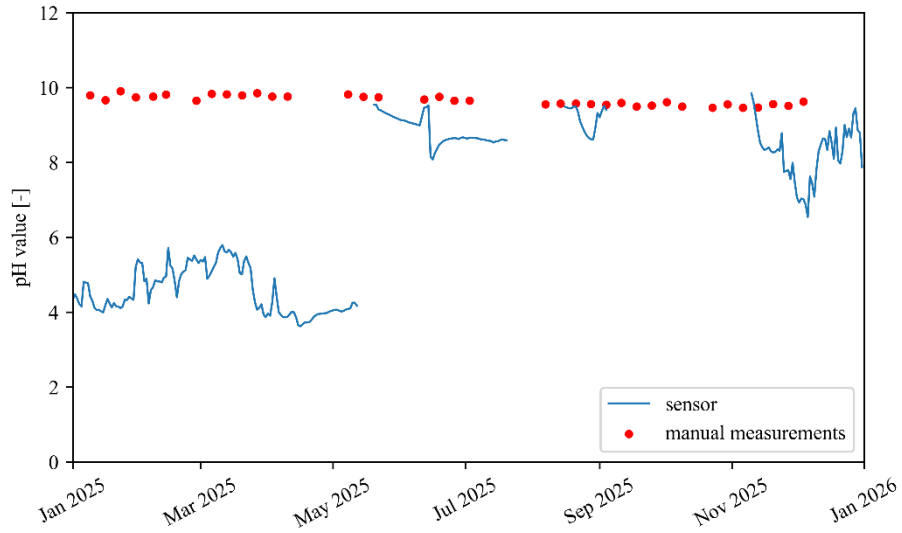


Figure 15: Water pH measurements in 2025. The blue curve illustrates continuous measurements from a sensor on site, while the red dots are manual measurements (extracting water from the storage).

11 Storage efficiency

The monthly charged and discharged energy, internal energy change, total heat loss, heat loss through the lid, and efficiency are documented in Table 4. It can be observed that the monthly efficiency ranged from 63% to 97%. However, these values are sensitive to the cut-off dates, and there is high uncertainty in the monthly heat loss calculation. The total efficiency for 2025 was 90%, which is slightly higher compared to 2024.

The heat loss through the lid is also mentioned in Table 4 and can be compared to the total heat loss. The heat loss through the lid was calculated using the measured lid heat flux and a lid area of 11000 m^2.

Table 4: Monthly charged and discharged energy, internal energy change, heat loss, and efficiency for 2025.

Period [2025]	$E_{charged}$ [MWh]	$E_{discharged}$ [MWh]	$\Delta E_{internal}$ [MWh]	$E_{loss, total}$ [MWh]	$E_{loss, lid}$ [MWh]	$E_{loss,ground}$ [MWh]	Efficiency [%]
January	4308	3535	321	452	113	339	89
February	2608	4177	-1709	140	96	44	97
March	4562	4398	-79	243	102	141	95
April	4713	2912	1457	343	95	248	89
May	4305	3551	417	337	96	241	91
June	1822	2493	-1001	330	88	242	88
July	2324	1022	934	368	87	281	74
August	207	1834	-1725	98	81	17	95
September	2799	560	1914	325	92	233	63
October	3106	2373	283	450	104	346	84
November	3231	3109	-201	323	107	216	91
December	2708	3662	-1175	221	111	110	94
Total	**36693**	**33626**	**-564**	**3630**	**1172**	**2458**	**90**

Compared to 2024, more energy was charged and discharged in 2025 (as indicated also by the increase in the storage cycles). The higher temperatures in the storage also led to slightly higher total heat loss for 2025. However, the heat loss toward the ground was slightly decreased in 2025 (approximately -1%), due to the higher ground temperatures compared to 2024.

12 Conclusion

This report presents an overview of the measurement results of the pit thermal energy storage (PTES) in Høje Taastrup for 2025. In general, the PTES had a comparable performance to the previous years, without any significant signs of degradation in its performance.

13 References

[1] PlanEnergi, "Design and Construction of the Pit Thermal Energy Storage in Høje Taastrup." [Online]. Available: https://planenergi.eu/wp-content/uploads/2024/01/FLEX_TES-Implementationreport_final_23.12.23.pdf

[2] I. Sifnaios, A. R. Jensen, and S. Furbo, "Høje Taastrup Pit Thermal Energy Storage: 2023 Measurement Report," 2024. doi: 10.11581/DTU.00000350.

[3] I. Sifnaios, A. R. Jensen, and S. Furbo, "Høje Taastrup Pit Thermal Energy Storage: 2024 Measurement Report," 2025. doi: https://doi.org/10.11581/5725831c-a697-4211-a049-34bc71025a50.

[4] G. M. Wallner, M. Povacz, R. Hausner, and R. W. Lang, "Lifetime modeling of polypropylene absorber materials for overheating protected hot water collectors," *Sol. Energy*, vol. 125, pp. 324–331, Feb. 2016, doi: 10.1016/j.solener.2015.12.035.